Tuning from frustrated magnetism to superconductivity in quasi-one-dimensional KCr$_3$As$_3$ through hydrogen doping

Keith M. Taddei [1,*] Liurukara D. Sanjeewa,[2] Bing-Hua Lei,[3] Yuhao Fu,[3] Qiang Zheng,[2] David J. Singh,[3] Athena S. Sefat,[2] and Clarina dela Cruz[1]

[1]*Neutron Scattering Division, Oak Ridge National Laboratory, Oak Ridge, Tennessee 37831, USA*
[2]*Materials Science and Technology Division, Oak Ridge National Laboratory, Oak Ridge, Tennessee 37831, USA*
[3]*Department of Physics and Astronomy, University of Missouri, Missouri 65211, USA*

We report the charge doping of KCr$_3$As$_3$ via H intercalation. We show that the previously reported ethanol bath deintercalation of K$_2$Cr$_3$As$_3$ to KCr$_3$As$_3$ has a secondary effect whereby H from the bath enters the quasi-one-dimensional Cr$_6$As$_6$ chains. Furthermore, we find that—contrary to previous interpretations—the difference between nonsuperconducting as-grown KCr$_3$As$_3$ samples and superconducting hydrothermally annealed samples is not a change in crystallinity but due to charge doping, with the latter treatment increasing the H concentration in the CrAs tubes, effectively electron doping the 133 compound. These results suggest another stoichiometry KH$_x$Cr$_3$As$_3$, that superconductivity arises from a suppressed magnetic order via a tunable parameter and paves the way for a charge-doped phase diagram in these materials.

Arguably the start of quantum materials, superconductors have suggested topological classifications, given rise to the resonating valence bond theory used in quantum spin liquids, and have formed the basis of numerous technologies in quantum information [1–6]. Yet unlike many of the topological quantum materials whose physics are understood but which struggle to find physical realizations, unconventional superconductors exist but have no settled microscopic theory, leaving their optimization unguided [3,7–10]. Instead, we rely on an empirical recipe derived from a surprisingly universal phase diagram where superconductivity is found near instabilities [11].

To refine this recipe and discriminate between possible mechanisms, it is useful to find new unconventional superconductors which are structurally simple, have few orders, and are easy to address theoretically (e.g., fewer relevant orbitals, lower dimensionality.) Much as the iron superconductors helped refine themes from the cuprates, a new family of superconductors A_2TM$_3$As$_3$ (A = Na, K, Cs, or Rb, TM = Cr or Mo, and $P\bar{6}m2$ symmetry) has begun offering insights, but helpfully via a quasi-one-dimensional structure [11–17]. Neutron scattering, nuclear magnetic resonance, Raman scattering, and density functional theory work have revealed both structural and magnetic instabilities—as seen in the iron-based superconductors [18–23]. However, in K$_2$Cr$_3$As$_3$, for instance, these orders break different symmetries, show no coupling, and suggest that only magnetism couples to superconductivity [18,19]. Additionally, evidence of Luttinger liquid physics, spin-triplet superconductivity, topological superconductivity, and a nodal gap function have emerged, indicating the broader novelty of this system [24–31]. Nonetheless,

its study has been inhibited by an extreme air sensitivity and lack of charge doped variants [32].

Promisingly, KCr$_3$As$_3$ (with $P6_3/m$ symmetry) addresses these issues with both a diminished electron count and stability in air. KCr$_3$As$_3$ (or "133" as opposed to "233" for K$_2$Cr$_3$As$_3$) is created by soaking 233 in ethanol, which ostensibly removes one K while retaining the quasi-one-dimensional CrAs tubes, and thus affords access to end members of a potential phase diagram [33]. Yet, results from KCr$_3$As$_3$ (and the broader ACr$_3$As$_3$ family) have proven contentious. Initially, it was reported as nonsuperconducting with spin-glass-like magnetism [16,33]. More recently, a postbath hydrothermal ethanol anneal was found to produce bulk superconductivity with nonmagnetic behavior [34,35]. Similarly, theory work has found conflict, with reports of long-range magnetic ground states, Fermi-surface nesting mediated superconductivity, and of a structural instability which precludes spin-mediated superconductivity [31,36,37].

Previously, crystalline disorder has been suggested to explain these conflicting results—in Ref. [34] it is argued that superconductivity arises in KCr$_3$As$_3$ upon postannealing due to an improvement of the crystallinity, while in theory work, Ref. [36] suggests its predicted magnetic order is not seen experimentally due to disorder in the physical material and Ref. [37] suggests that similar to K$_2$Cr$_3$As$_3$ the predicted structural instability may have no long-range coherence [19]. In attempting to sort through these possibilities, we stumbled upon an unexpected but useful origin to these discrepancies.

Here, we report a systematic study of synthesis reactions for KCr$_3$As$_3$ using neutron and x-ray diffraction together with density functional theory (DFT). We reveal a previously missed effect of the ethanol bath whereby H is unavoidably intercalated into the CrAs tubes, leading to a KH$_x$Cr$_3$As$_3$ stoichiometry. We show that H concentration is controllable

*Corresponding author: taddeikm@ornl.gov
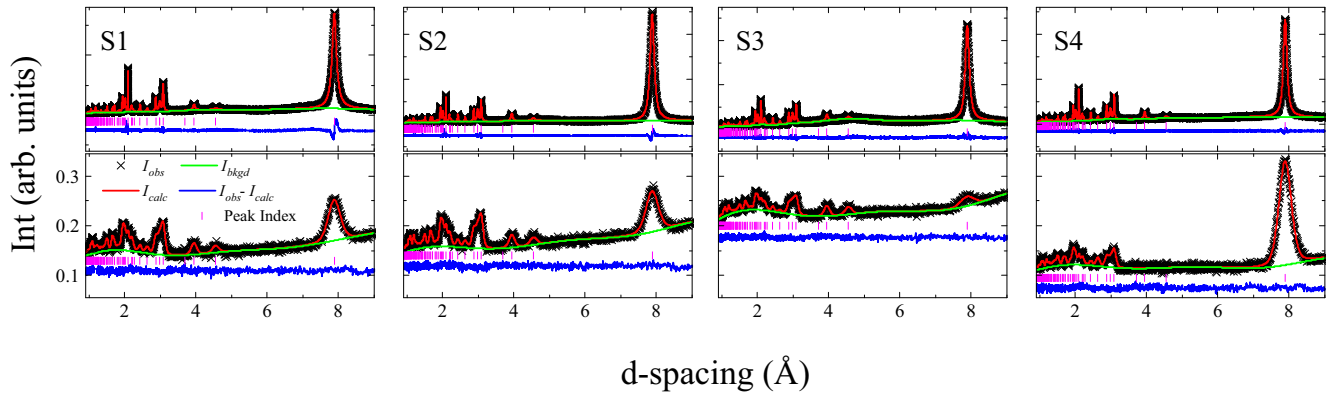
FIG. 1. Room-temperature x-ray (top row) and neutron (bottom row) powder diffraction patterns for the four KCr_3As_3 samples plotted with the results of Rietveld refinements for H and D containing models. The neutron diffraction data were collected using identical sample mass, neutron exposures, and sample containers, and thus the scattered neutron intensity is directly comparable between samples.

and that the difference between nonsuperconducting spin-glass and nonmagnetic superconducting samples is not in the sample crystallinity but in the amount of H intercalated. Our DFT work suggests that the $KH_xCr_3As_3$ structure is stable, electron doped relative to KCr_3As_3, and exhibits an electronic structure more similar to $K_2Cr_3As_3$ than KCr_3As_3. Additionally, we find that the H stabilizes the $P6_3/m$ structure and places the compound proximate to an antiferromagnetic instability. These results lead to the exciting possibility of continuously tuning $KH_xCr_3As_3$ from a spin glass to a superconductor via charge doping with H—the long sought after tuning parameter. Furthermore, this shifts interest to another air stable compound, opening up this system for widespread study. More contemplatively, it offers a realization of a frustrated magnetic to superconducting transition in a quasi-one-dimensional (Q1D) system which has long been suggested as a potential recipe for spin-liquid physics [38,39].

Neutron powder diffraction (NPD) data were collected using the HB-2A and NOMAD diffractometers of Oak Ridge National Laboratory's High Flux Isotope Reactor and Spallation Neutron Source [40–42]. High-resolution synchrotron x-ray powder diffraction (XRD) data were collected at beamline 11BM-B of the Advanced Photon Source at Argonne National Laboratory. Structural analysis was performed using the Rietveld method as implemented in the FULLPROF, GSAS, and EXPGUI software suites [see Supplemental Material (SM) [43] for more details] [44–47]. DFT calculations were performed using projector-augmented plane-wave method and checked using the general potential linearized augmented plane-wave method as implemented in VASP and WIEN2K, respectively [48–52]. Phonon spectrums were calculated using the PHONOPY code [53]. For more details on the calculations, see the SM [43] and references contained therein [54].

To study how the synthesis procedures effect the measured properties, we synthesized powder samples following the methodologies reported by Bao *et al.* in Ref. [33] and Mu *et al.* in Ref. [34]. Thus three samples were used for initial characterization: (S1) as grown from an ethanol bath, (S2) with a postbath vacuum anneal, and (S3) with both postbath hydrothermal and vacuum anneals [a fourth sample (S4) was also grown and will be discussed later in this

text]. Susceptibility measurements show we were successful in reproducing the previously reported change in properties with S1 and S2 being trace superconductors with spin-glass properties (identified here as in Ref. [33]) and S3 showing bulk superconductivity (see SM [43]).

Previously, the change in properties was attributed to the postbath annealings' effects on the crystallinity of the sample. Ostensibly, the more crystalline annealed samples hosted superconductivity which was otherwise destroyed by disorder in the as-grown samples [34]. To test this assertion, NPD and XRD data were collected and are shown along with the best fit results of Rietveld refinements in Fig. 1. We note that even visually, the main qualitative difference between the samples is not in the peak shape but in the background to signal ratio. Specifically, in the NPD data the bulk superconducting S3 has a remarkably larger background to signal ratio than any other sample.

To qualitatively check the crystallographic properties, the NPD and XRD were used together for Rietveld refinements. From this analysis, the lattice parameters and measures of strain, crystallinity, and grain size can be assessed (plotted as a function of sample number along with the 233 compound labeled as sample 5 in Fig. 2). Considering the extracted anisotropic microscopic strain parameters (L_{nn} where $n = 1, 2, 3$ correspond to the a, b, and c lattice directions, respectively) and L_x (which is proportional to the inverse of the crystallite size), little difference is seen in these terms between samples, indicating similar crystalline properties. Compared to the broadening parameters determined in previous work on the 233 compound [18], it is seen that generally the deintercalation process leaves the 133 material with poor crystallinity. However, it is not significantly improved upon either vacuum or hydrothermal annealing, in contrast with previous reports which did not compare qualitative measures of the crystallinity [34].

Looking at the crystal parameters, a clear trend relative to the superconducting volume fraction is seen [Fig. 2(b)]. Both the a and c lattice parameters dilate between the trace (S2) and bulk (S3) superconducting samples by 0.1% and 0.4%, respectively, leading to a >0.4% change in the unit cell volume [Fig. 2(b)]. On the other hand, between S1 and S2 no such
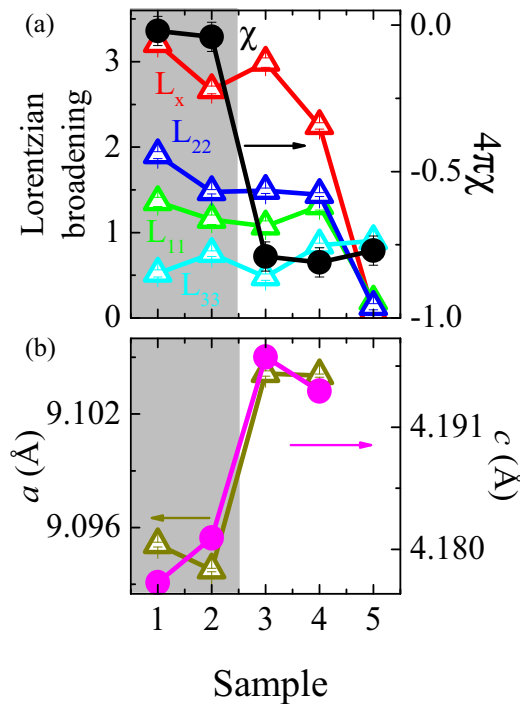
FIG. 2. (a) Lorentzian broadening terms in the GSAS profile fitting function including three terms for microstrain along the unit cell directions (L_{11}, L_{22}, and L_{33}) and one term (L_x) for particle size broadening. This latter is proportional to the inverse of the particle size. The superconducting volume fraction determined at 1.5 K is overplotted with sample 5 denoting the pure 233 compound. (b) The refined a and c lattice parameters. Throughout the figure, data with the scale on the left axis are plotted with open triangles while data with the scale on the right axis are plotted as solid circles. The gray shaded region denotes samples with only trace superconductivity.

change is seen, with only a small ∼0.1% change in volume. These results are unexpected: If the postannealing treatments improve the crystallinity, the peak broadening terms should decrease and the unit cell relax—our data directly contradict this [55,56]. Therefore, we searched for a different explanation for the change in properties between the trace and bulk superconducting samples.

Noting that the background to signal increase is only seen in NPD and is exacerbated by the hydrothermal anneal, we posit the presence of H in the samples. H is nearly invisible to x rays but has a large incoherent cross section to neutrons ($\sigma_{H_{inc}} \sim 80.26b$) [57]. This manifests as a large background which increases with d spacing and could explain the difference between the XRD and NPD patterns [58]. As such, any H in KCr_3As_3 would be missed in XRD and energy dispersive x-ray spectroscopy elucidating why such a feature has not been seen in previous structural work [16,33–35]. We propose several mechanisms which would introduce H to the samples during the ethanol baths: a remnant minority organic compound not removed during washing, substitution onto the K site, or intercalation into the 133 structure. Of these scenarios the latter two provide an explanation for the increase in background upon the hydrothermal anneal assuming the process either forces more H into the material through higher temperature, pressure, or a longer exposure to ethanol.

To discriminate between these scenarios, a sample of 133 was grown following the procedure of S3 but using fully deuterated ethanol in all steps. The resulting sample (S4) shows similar superconducting properties to S3 (see SM [43]), indicating that the use of deuterated ethanol does not significantly change the sample properties. Deuterium (D) does not have the large incoherent cross section of H ($\sigma_{D_{inc}} \sim 2.05b$) and so does not add as much background scattering. Furthermore, it has a large coherent cross section ($\sigma_{D_{coh}} \sim 7.6b$), allowing for reliable structural model refinements (the coherent cross sections of K, Cr, As, and H are 1.69b, 1.66b, 5.44b, and 1.76b, respectively) [57]. Therefore, if H is intercalated or substitutes for K, using D would allow for structure solution and composition determination through changes in peak intensities, else if the H background comes from remnant organic compounds, the background will be reduced in S4 but no other changes should occur.

The XRD and NPD of S4 are shown in Fig. 1. While the XRD looks similar to the other samples, the NPD exhibits a nearly 50% reduction in background (compared to S3) as well as a change in peak intensities where peaks at 3.9 and 4.6 Å [the (020) and (110) reflections, respectively] become background equivalent. The background reduction confirms the presence of H in the samples (rather than, for instance, the background arising from amorphous parts of the sample) while the change in peak intensities indicates that the H and D are incorporated into the 133's crystal structure rather than existing as remnant organic compounds.

To determine where D is incorporated, Rietveld analysis was performed using the NPD. Since the D containing sample shows a reduction in peak intensity but not the appearance of new peaks, the original $P6_3/m$ crystal symmetry was used and Rietveld refinements were performed trying models containing D on all of $P6_3/m$'s special Wyckoff positions. Of these, only models with D on the 2b (0,0,0) site reproduced the observed intensities as shown in Fig. 1, leading to high-quality fits with small residuals (see SM for fit parameters [43]).

The new structural model is shown in Fig. 3. In it, D is intercalated into the center of the CrAs tubes between the stacked CrAs layers, creating a chain of D centered in each tube. We find no evidence of K vacancies or of D substitution on the K site. However, our refinements show the D site is only partially occupied with a refined occupancy of 65%.

With the location in hand, Rietveld refinements were tried using similar models for S1, S2, and S3—this is possible since H has a coherent cross section which is on the order of both K and Cr. Starting with S3, our refinements show agreement with S4, with a similar occupancy of ∼71%. This corroborates that the synthesis procedure and resulting material is insensitive to the change from H to D. On the other hand, S1 and S2 are found to have significantly less H than S3 and S4. Both the S1 and S2 models refine to have ∼35% H. As all samples show intercalated H—even the nonbulk superconductors—we revise the chemical formula of KCr_3As_3 to $KH_xCr_3As_3$, explicitly reflecting the H content and its variability.

These results elucidate the effects of the different reaction stages. During the room-temperature bath, K is deintercalated from the 233 starting material as reported previously, however, some H from the bath also intercalates into the CrAs tubes
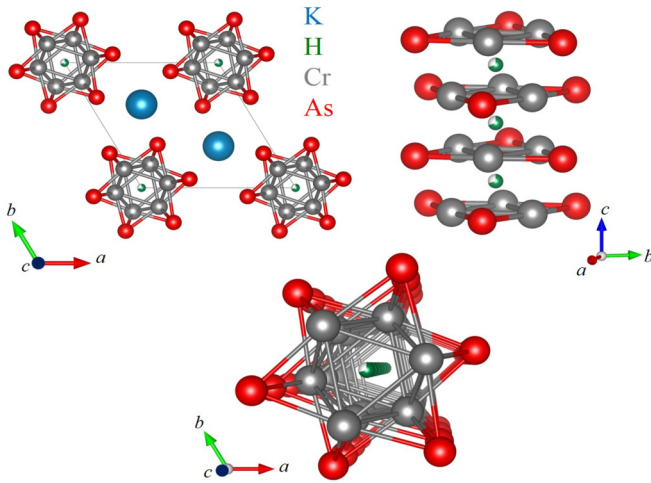
FIG. 3. $KH_xCr_3As_3$ structure as viewed along the c axis, perpendicular to the c axis, and along the CrAs tubes. K, H, Cr, and As atoms are denoted by turquoise, dark green, gray, and red spheres, respectively. The partial occupancy of the H site is indicated by a wedge of white in the H atom surface.

FIG. 4. DFT calculated band structure for (left) the KCr_3As_3 and (right) $KHCr_3As_3$ stoichiometries.

between the CrAs layers. Whether this occurs to charge compensate for the deintercalated K is not known and should be the interest of future work—although this may be indicated by the inability to synthesize KCr_3As_3 directly from solid state methods [33,34]. The similarities both in crystallinity and H content of S1 and S2 suggest that vacuum annealing neither improves the sample quality nor vents the intercalated H. This latter result suggests the stability of $KH_xCr_3As_3$ at least up to the annealing temperatures used in this work. Upon hydrothermal annealing, more H intercalates into the structure, bringing the concentration from ~35% to ~65%–71%.

It is this latter effect which appears to induce superconductivity in $KH_xCr_3As_3$. As discussed, no change in crystallinity is seen between bulk and trace superconducting samples but rather a change in the lattice parameters. We can now ascribe this to an increase in the amount of H intercalated into the CrAs tubes. Beyond causing the unit cell to expand, the intercalated H should also affect the charge count, however, the chemistry of H is incredibly flexible and its electronic contribution is not evident from the diffraction data [59,60].

To study $KH_xCr_3As_3$'s energetics and electronic structure, DFT calculations were performed using the theoretical $x = 0$ and $x = 1$ stoichiometries. Calculations for $KHCr_3As_3$'s formation energy relative to KCr_3As_3 and H_2 gas found a negative formation energy of 92 kJ/mol H_2—similar to that of other stable hydrides such as MgH_2—indicating the intercalated structure is energetically favorable (see SM for more details) [43]. Calculations of $KHCr_3As_3$'s band structure (Fig. 4) show that the intercalated H raises the Fermi energy (E_F) and causes only modest distortions to the bands near E_F. Therefore, we can say that in $KHCr_3As_3$, H has metallic bonding and acts as an electron donor. As shown, it increases the electron count such that the electronic structures (and the Fermi surface—see SM [43]) are more similar to $K_2Cr_3As_3$ than the pure KCr_3As_3, suggesting similar electronic behavior.

Inspired by previous reports of instabilities, we also performed calculations of the phonon spectrum and proximity
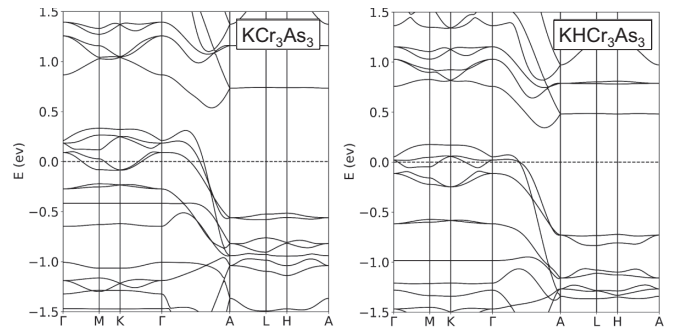
to magnetic instabilities [31,36,37,61]. Considering the predicted structural instability, our calculations show no unstable phonon modes and relatively high energy nearly dispersionless H modes, suggesting that H removes the phonon instability, leaving $KHCr_3As_3$ structurally stable [62]. Finally, we consider the hydride's proximity to magnetic instabilities. Previously, KCr_3As_3 has been suggested to either have a magnetic ground state which is frustrated by disorder, or no magnetic ground state due to a structural instability which removes favorable nesting conditions [36,37]. For $KHCr_3As_3$ we find weak itinerant instabilities to both ferromagnetic and antiferromagnetic A-type magnetic orders with a slight preference for the latter. However, we also find both itinerancy and low-energy scales, suggesting that the magnetic order could easily be suppressed to a paramagnetic state with spin fluctuations by quantum fluctuations such as the case of Ni_3Ga [63]. This last result is quite interesting as it restores the possibility of a spin-driven pairing mechanism which had previously been discounted in Ref. [37].

These combined results suggest that superconductivity arises in $KH_xCr_3As_3$ upon electron doping, a process which until now has been achieved unintentionally during the hydrothermal anneal. In this scenario, the underdoped $KH_{0.35}Cr_3As_3$ is a nonsuperconducting spin-glass phase as reported by Bao *et al.* [33]. Upon electron doping to $KH_{0.65}Cr_3As_3$ via hydrothermal annealing, the spin-glass phase is suppressed and the material becomes a bulk superconductor with T_c ~5 K, as reported by Mu *et al.* [34]. This has multiple significant implications: (i) The intercalated CrAs systems inhabit a familiar phase space where superconductivity arises out of a suppressed magnetic state, (ii) the possibility of creating the elusive charge doped phase diagram for the intercalated CrAs ($KH_xCr_3As_3$ as well as the Rb and Cs analogs), (iii) the need to revisit previous *ab initio* calculations on the ACr_3As_3 materials which were based on the hydrogen-free 133 stoichiometry, and (iv) an avenue to study how superconductivity arises from a frustrated magnetic state in a quasi-one-dimensional system by charge doping, a concept which has long held interest for spin- and Luttinger-liquid physics [38,39]. As an additional point of interest, one of the significant impediments to the study of the intercalated CrAs materials to this point has been the 233 stoichiometry's extreme air sensitivity. With this work, we show a clear path forward to study interactions between magnetic and superconducting orders in the air stable 133

stoichiometry, alleviating this barrier. Our results layout a rich path of future work, not least of which will be to gain fine control of the H content through the synthesis procedures.

Note added. Recently, we became aware of two articles that have been published which further encourage work towards a $KH_xCr_3As_3$ phase diagram. One describes the complex chemistry leading to the H intercalation [64] while the other examines the calculated band structures of the system with and without H to predict the existence of a Lifshitz transition at some critical H concentration [65].

The Department of Energy will provide public access to these results of federally sponsored research in accordance with the DOE Public Access Plan [66].

The US Government retains, and the publisher, by accepting the article for publication, acknowledges that the US Government retains a nonexclusive, paid-up, irrevocable, worldwide license to publish or reproduce the published form of this manuscript or allow others to do so for US Government purposes.

---

[1] J. Bednorz and K. Müller, Z. Phys. B **64**, 189 (1986).

[2] P. Anderson, Science **235**, 1196 (1987).

[3] X.-G. Wen, Rev. Mod. Phys. **89**, 041004 (2017).

[4] Y. Nakamura, Y. Pashkin, and J. Tsai, Nature (London) **398**, 786 (1999).

[5] N. Read and D. Green, Phys. Rev. B **61**, 10267 (2000).

[6] J. Linder and J. Robinson, Nat. Phys. **11**, 307 (2015).

[7] R. Fernandes and A. Chubukov, Rep. Prog. Phys. **80**, 014503 (2016).

[8] S. Lee, P. Sharma, A. Lima-Sharma, W. Pan, and T. Nenoff, Chem. Mater. **31**, 26 (2019).

[9] L. Balents, Nature (London) **464**, 199 (2010).

[10] M. R. Norman, Science **332**, 196 (2011).

[11] D. Basov and A. Chubukov, Nat. Phys. **7**, 272 (2011).

[12] J. M. Allred, K. M. Taddei, D. E. Bugaris, M. J. Krogstad, S. H. Lapidus, D. Y. Chung, H. Claus, M. G. Kanatzidis, D. E. Brown, J. Kang, R. M. Fernandes, I. Eremin, S. Rosenkranz, O. Chmaissem, and R. Osborn, Nat. Phys. **12**, 493 (2016).

[13] J.-K. Bao, J.-Y. Liu, C.-W. Ma, Z.-H. Meng, Z.-T. Tang, Y.-L. Sun, H.-F. Zhai, H. Jiang, H. Bai, C.-M. Feng, Z.-A. Xu, and G.-H. Cao, Phys. Rev. X **5**, 011013 (2015).

[14] Q.-G. Mu, B.-B. Ruan, B.-J. Pan, T. Liu, J. Yu, K. Zhao, G.-F. Chen, and Z.-A. Ren, Phys. Rev. Materials **2**, 034803 (2018).

[15] Q.-G. Mu, B.-B. Ruan, K. Zhao, B.-J. Pan, T. Liu, L. Shan, G.-F. Chen, and Z.-A. Ren, Sci. Bull. **63**, 952 (2018).

[16] Z.-T. Tang, J. Bao, Y. Liu, H. Bai, H. Jiang, H.-F. Zhai, C.-M. Feng, Z.-A. Xu, and G.-H. Cao, Sci. China Mater. **58**, 543 (2015).

[17] K. Zhao, Q.-G. Mu, T. Liu, B.-J. Pan, B.-B. Ruan, L. Shan, G.-F. Chen, and Z.-A. Ren, arXiv:1805.11577.

[18] K. M. Taddei, Q. Zheng, A. S. Sefat, and C. de la Cruz, Phys. Rev. B **96**, 180506(R) (2017).

[19] K. M. Taddei, G. Xing, J. Sun, Y. Fu, Y. Li, Q. Zheng, A. S. Sefat, D. J. Singh, and C. de la Cruz, Phys. Rev. Lett. **121**, 187002 (2018).

[20] H. Z. Zhi, T. Imai, F. L. Ning, J.-K. Bao, and G.-H. Cao, Phys. Rev. Lett. **114**, 147004 (2015).

[21] W.-L. Zhang, H. Li, D. Xia, H. W. Liu, Y.-G. Shi, J. L. Luo, J. Hu, P. Richard, and H. Ding, Phys. Rev. B **92**, 060502(R) (2015).

[22] X.-X. Wu, C.-C. Le, J. Yuan, H. Fan, and J.-P. Hu, Chin. Phys. Lett. **32**, 057401 (2015).

[23] H. Jiang, G. Cao, and C. Cao, Sci. Rep. **5**, 16054 (2015).

[24] M. D. Watson, Y. Feng, C. W. Nicholson, C. Monney, J. M. Riley, H. Iwasawa, K. Refson, V. Sacksteder, D. T. Adroja, J. Zhao, and M. Hoesch, Phys. Rev. Lett. **118**, 097002 (2017).

[25] Y. Shao, X. Wu, L. Wang, Y. Shi, J. Hu, and J. Luo, Europhys. Lett. **123**, 57001 (2018).

[26] Y. Liu, J.-K. Bao, H.-K. Zuo, A. Ablimit, Z.-T. Tang, C.-M. Feng, Z.-W. Zhu, and G.-H. Cao, Sci. China: Phys., Mech. Astron. **59**, 657402 (2016).

[27] D. T. Adroja, A. Bhattacharyya, M. Telling, Y. Feng, M. Smidman, B. Pan, J. Zhao, A. D. Hillier, F. L. Pratt, and A. M. Strydom, Phys. Rev. B **92**, 134505 (2015).

[28] J. Sun, Y. Jiao, C. Yang, W. Wu, C. Yi, B. Wang, Y. Shi, J. Luo, Y. Uwatoko, and J. Cheng, J. Phys.: Condens. Matter **29**, 455603 (2017).

[29] S.-M. Huang, C.-H. Hsu, S.-Y. Xu, C.-C. Lee, S.-Y. Shiau, H. Lin, and A. Bansil, Phys. Rev. B **97**, 014510 (2018).

[30] J. Yang, Z. T. Tang, G. H. Cao, and G.-q. Zheng, Phys. Rev. Lett. **115**, 147002 (2015).

[31] L.-D. Zhang, X. Zhang, J.-J. Hao, W. Huang, and F. Yang, Phys. Rev. B **99**, 094511 (2019).

[32] Q. Mu, B. Ruan, B. Pan, T. Liu, K. Zhao, G. Chen, and Z. Ren, J. Phys.: Condens. Matter **31**, 225701 (2019).

[33] J.-K. Bao, L. Li, Z.-T. Tang, Y. Liu, Y.-K. Li, H. Bai, C.-M. Feng, Z.-A. Xu, and G.-H. Cao, Phys. Rev. B **91**, 180404(R) (2015).

[34] Q.-G. Mu, B.-B. Ruan, B.-J. Pan, T. Liu, J. Yu, K. Zhao, G.-F. Chen, and Z.-A. Ren, Phys. Rev. B **96**, 140504(R) (2017).

[35] T. Liu, Q.-G. Mu, B.-J. Pan, J. Yu, B.-B. Ruan, K. Zhao, G.-F. Chen, and Z.-A. Ren, Europhys. Lett. **120**, 27006 (2017).

[36] C. Cao, H. Jiang, X.-Y. Feng, and J. Dai, Phys. Rev. B **92**, 235107 (2015).

[37] G. Xing, L. Shang, Y. Fu, W. Ren, X. Fan, W. Zheng, and D. Singh, Phys. Rev. B **99**, 174508 (2019).

[38] M. Sigrist, T. M. Rice, and F. C. Zhang, Phys. Rev. B **49**, 12058 (1994).

[39] T. M. Rice, S. Gopalan, and M. Sigrist, Europhys. Lett. **23**, 445 (1993).

[40] S. Calder, K. An, R. Boehler, C. Dela Cruz, M. Frontzek, M. Guthrie, B. Haberl, A. Huq, S. A. Kimber, J. Liu *et al.*, Rev. Sci. Instrum. **89**, 092701 (2018).

[41] M. T. McDonnell, D. P. Olds, K. L. Page, J. C. Neufeind, M. G. Tucker, J. C. Bilheux, W. Zhou, and P. F. Peterson, Acta Crystallogr., Sect. A **73**, a377 (2017).

[42] J. Neuefeind, M. Feygenson, J. Carruth, R. Hoffmann, and K. K. Chipley, Nucl. Instrum. Methods **287**, 68 (2012).

[43] See Supplemental Material at http://link.aps.org/supplemental/10.1103/PhysRevB.100.220503 for details pertaining to sample synthesis, diffraction data collection, Rietveld refinements, and a more in-depth discussion of the DFT results.

[44] J. Rodríguez-Carvajal, Physica B (Amsterdam) **192**, 55 (1993).

[45] A. Larson and R. Von Dreele, Los Alamos National Laboratory Report No. LAUR 86-748, 2004.

[46] R. B. Von Dreele, J. D. Jorgensen, and C. G. Windsor, J. Appl. Crystallogr. **15**, 581 (1982).

[47] L. W. Finger, D. E. Cox, and A. P. Jephcoat, J. Appl. Crystallogr. **27**, 892 (1994).

[48] G. Kresse and D. Joubert, Phys. Rev. B **59**, 1758 (1999).

[49] G. Kresse and J. Furthmüller, Phys. Rev. B **54**, 11169 (1996).

[50] J. P. Perdew, K. Burke, and M. Ernzerhof, Phys. Rev. Lett. **77**, 3865 (1996).

[51] D. Singh and L. Nordström, *Planewaves, Pseudopotentials and the LAPW Method*, 2nd ed. (Springer, Berlin, 2006).

[52] P. Blaha, K. Schwarz, G. Madsen, D. Kvasnicka, and J. Luitz, *WIEN2k, An Augmented Plane Wave + Local Orbitals Program for Calculating Crystal Properties* (Technische Universität Wien, Wien, 2001).

[53] A. Togo and I. Tanaka, Scr. Mater. **108**, 1 (2015).

[54] A. Subedi, Phys. Rev. B **92**, 174501 (2015).

[55] T. Forrest, P. Valdivia, C. Rotundu, E. Bourret-Courchesne, and R. Birgeneau, J. Phys.: Condens. Matter **28**, 115702 (2016).

[56] G. Becht, J. Vaughey, R. Britt, C. Eagle, and S.-J. Hwu, Mater. Res. Bull. **43**, 3389 (2008).

[57] V. Sears, Neutron News **3**, 26 (2006).

[58] L. Temleitner, A. Stunault, G. J. Cuello, and L. Pusztai, Phys. Rev. B **92**, 014201 (2015).

[59] M. Gupta, R. P. Gupta, and D. J. Singh, Phys. Rev. Lett. **95**, 056403 (2005).

[60] H. Khan and C. Raub, J. Less-Common Met. **49**, 399 (1976).

[61] Y. Feng, X.-W. Zhang, Y.-Q. Hao, A. D. Hillier, D. T. Adroja, and J. Zhao, Phys. Rev. B **99**, 174401 (2019).

[62] J. Rowe, J. Rush, H. Smith, M. Mostoller, and H. Flotow, Phys. Rev. Lett. **33**, 1297 (1974).

[63] A. Aguayo, I. I. Mazin, and D. J. Singh, Phys. Rev. Lett. **92**, 147201 (2004).

[64] J.-J. Xiang, Y.-L. Yu, S.-Q. Wu, B.-Z. Li, Y.-T. Shao, Z.-T. Tang, J.-K. Bao, and G.-H. Cao, Phys. Rev. Materials **3**, 114802 (2019).

[65] S.-Q. Wu, C. Cao, and G.-H. Cao, Phys. Rev. B **100**, 155108 (2019).

[66] http://energy.gov/downloads/doe-public-access-plan